Parametric Refinement and Low-Cost In-House Photolithographic Fabrication of a Planar Log Spiral Antenna for Broadband RF Energy Harvesting

Nurulhalim Bin Hassim[1]*, Mohd. Hariz Iskandar[1]

[1] Centre for Telecommunication Research and Innovation, Fakulti Teknologi dan Kejuruteraan Elektronik dan Komputer, Universiti Teknikal Malaysia Melaka (UTeM), Durian Tunggal, Melaka 76100, Malaysia

DOI: https://doi.org/10.47772/IJRISS.2026.101000145

Received: 11 October 2026; Accepted: 16 October 2026; Published: 30 October 2026

ABSTRACT

Planar log spiral antennas are attractive receivers for ambient radio frequency (RF) energy harvesting because their equiangular geometry supports broadband, nearly frequency-independent operation. How the closed-form spiral equations are turned into a board-sized, manufacturable layout is rarely documented, particularly below 3 GHz, where the spiral grows rapidly with every turn. This paper is a companion to a previously reported ultra-wideband log spiral antenna and documents the design-to-prototype workflow behind it. Radius bounds for a 0.5–3 GHz band are derived from the active-region criterion and used to check an analytical seed geometry ($k = 1.31$ mm, $\alpha = 0.50$, $\delta = 90°$, $N = 1.5$). Full-wave refinement in CST Studio Suite 2020 produced a geometry ($k = 1.37$ mm, $\alpha = 0.42$, $\delta = 120°$, $N = 1.8$) whose per-turn radial expansion falls from 23.1 to 14.0 and whose arm terminations fit a 300 × 150 × 1.6 mm FR-4 board, while its 158 mm outer extent still exceeds the 95.5 mm required for the lower band edge. Widening the arm angle moves the input impedance below the self-complementary value toward the simulated 80 Ω, which explains the near-constant −12 to −14 dB simulated reflection floor. The prototype was produced with an inkjet-printed photomask, 120 s UV exposure, ferric chloride spray etching and a soldered SMA feed, using only teaching-laboratory equipment. The previously reported measurements (minimum S11 of −32 dB and minimum VSWR of 1.06) are summarised to confirm the workflow, which is offered as a reproducible template for low-cost harvesting antennas; next steps in simulation, matching, rectification and masking are outlined.

Keywords - Log spiral antenna, parametric design, self-complementary antenna, photolithographic PCB fabrication, RF energy harvesting, FR-4 substrate, CST Studio Suite.

INTRODUCTION

Ambient radio frequency (RF) energy harvesting converts electromagnetic energy radiated by broadcast, cellular and wireless-network transmitters into usable DC power, offering a route to battery-free or battery-assisted wireless sensors and Internet-of-Things (IoT) nodes. A harvesting front end, or rectenna, combines a receiving antenna with a matching network and a rectifier, and the antenna is the first element that determines how much of the sparse ambient power density reaches the diode [1]. Because ambient power is distributed across several bands rather than concentrated at one frequency, broadband receiving antennas that cover the 0.5–3 GHz region, which contains the UHF broadcast, GSM900, GSM1800, 3G/4G and 2.4 GHz Wi-Fi allocations, are of particular interest.

Several broadband geometries have been explored for this purpose. El Khosht et al. [2] built a foldable textile Archimedean spiral and related its upper and lower operating frequencies to the inner and outer radii through $r = c/2\pi f$. Miao et al. [3] simulated a log spiral antenna integrated with an extended hemispherical lens and reported an almost constant input impedance over a very wide band, with the cut-off frequencies set by the outer and inner diameters. Mandal and Giri [4] compared patch, Archimedean, square and hexagonal spirals

for 0.2–2.4 GHz harvesting and highlighted the substrate area left unused by circular geometries. Kumar et al. [5] reported a triangular-element log-periodic dipole array with VSWR below 2 from 570 to 2750 MHz and an almost flat gain of about 7.2 dBi, while Gangwar and Tissier [6] optimised the inner radius, expansion coefficient and number of turns of a modified log-periodic spiral on 1.6 mm FR-4 and added split-ring resonators to widen its bandwidth. At circuit level, Jabbar et al. [7] showed that Villard voltage multipliers can convert harvested RF power into DC, provided the antenna is properly matched to the rectifier.

Most of these studies report final dimensions but say little about how the analytical spiral parameters were translated into a geometry that fits a practical board, or how the prototype was manufactured. For log spirals this gap matters, because the radius grows exponentially with angle: a geometry that satisfies the lower-frequency requirement can quickly outgrow the available substrate, while the turns near the feed become dense and demanding to reproduce.

The antenna discussed here was first reported in [8], which presented its simulated and measured reflection, VSWR and far-field performance; both works derive from the undergraduate project in [9]. The present paper reports no new prototype or measurements. Instead, it documents the steps that [8] did not cover: (i) closed-form radius bounds and geometric checks for the 0.5–3 GHz target; (ii) the evolution from the analytical seed parameters listed in [8] to the refined parameters actually simulated and fabricated, together with an impedance-based interpretation of that refinement; (iii) the in-house photolithographic fabrication process and its parameters; and (iv) a consolidated verification summary in which all measured values are attributed to [8].

DESIGN METHODOLOGY

The workflow is summarised in Fig. 1. It proceeds from analytical design to full-wave refinement and then to fabrication and test, with a single feedback loop in which the spiral parameters are adjusted until both the reflection target and the board-size constraint are met.

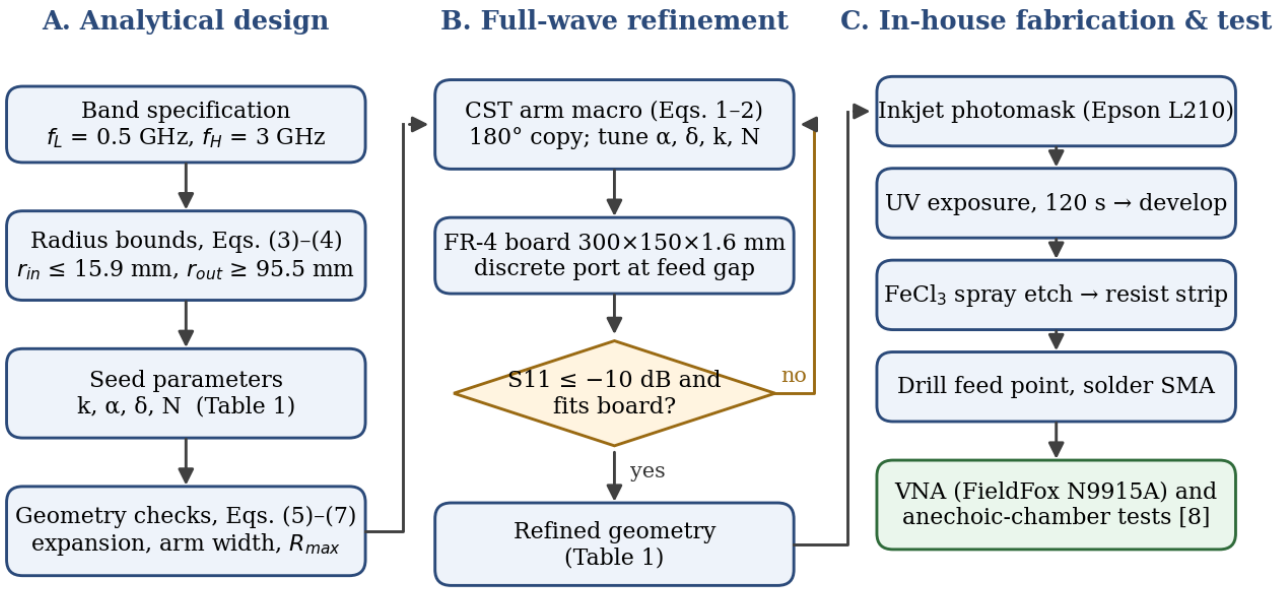

Fig. 1. Design-to-prototype workflow used for the log spiral antenna

Spiral geometry

Each arm of the planar equiangular spiral [10] is bounded by two curves of the same family, offset in angle by δ:

$$r_A(\varphi) = ke^{\alpha\varphi} \quad (1)$$

$$r_B(\varphi) = ke^{\alpha(\varphi-\delta)} \quad (2)$$

Here k is the initial radius, α the growth rate and φ the winding angle, which runs from 0 to 2πN for an arm of N turns. The second arm is identical and rotated by 180°. In the CST "Planar Logarithmic Spiral" macro these quantities appear directly as the initial radius, alpha, delta and number of turns; the macro's 5° "phi-increment" is only the angular step used to sample the spline and is not a design variable.

Band-limiting radii

A spiral radiates efficiently in the active region whose circumference is about one wavelength [10]. The innermost radius therefore limits the highest frequency, and the outermost radius the lowest, giving the bounds used in [2]:

$$r_{in} \leq \frac{c}{2\pi f_H} \quad (3)$$

$$r_{out} \geq \frac{c}{2\pi f_L} \quad (4)$$

With $c = 3 \times 10^8$ m/s, $f_H = 3$ GHz and $f_L = 0.5$ GHz, the spiral must start within $r_{in} = 15.9$ mm of the feed and must extend to at least $r_{out} = 95.5$ mm.

Geometric checks

Three derived quantities make the compactness trade-off explicit. The radial expansion per turn ε and the ratio ρ between the two edges of an arm follow from (1) and (2), and the arm terminates between the radii R_B and R_{max}:

$$\varepsilon = e^{2\pi\alpha}, \qquad \rho = \frac{r_A}{r_B} = e^{\alpha\delta} \quad (5)$$

$$R_{max} = ke^{2\pi N\alpha} \quad (6)$$

$$R_B = ke^{\alpha(2\pi N-\delta)} \quad (7)$$

A large ε means that each added turn multiplies the antenna size, which is the main practical drawback of log spirals noted in [9]. ρ sets the arm width, and R_{max} must exceed r_{out} while still fitting the available board.

Input impedance and matching

When δ = 90°, metal and slot occupy equal angular sectors and the two-arm spiral is self-complementary. Its input impedance is then fixed by Babinet's principle [11], [12], lying between the free-space value of 188 Ω and the dielectric half-space limit:

$$Z_{sc} \approx \frac{60\pi}{\sqrt{\varepsilon_{eff}}}, \qquad 1 \leq \varepsilon_{eff} \leq \frac{\varepsilon_r + 1}{2} \quad (8)$$

For FR-4 ($\varepsilon_r = 4.3$) the lower limit is about 116 Ω. When the antenna is fed from a 50 Ω port, the mismatch is quantified by the reflection coefficient and VSWR:

$$\Gamma = \frac{Z_{in} - Z_0}{Z_{in} + Z_0}, \qquad VSWR = \frac{1 + |\Gamma|}{1 - |\Gamma|} \quad (9)$$

Full-wave model

The model was built in CST Studio Suite 2020 (Fig. 2). The first arm was generated with the logarithmic

spiral macro using a 35 µm copper thickness, and the second arm was produced by a 180° rotational copy about the z-axis, which guarantees the point symmetry needed for a balanced feed. The arms sit on a 300 × 150 × 1.6 mm FR-4 (lossy) substrate taken from the CST library (ε_r = 4.3, tan δ = 0.025), with no ground plane. A discrete port was placed between the edge centres of the two inner arm terminals, which are 1.14 mm apart. The port impedance was set to 50 Ω to represent the SMA connector, and open boundaries with the time-domain solver were used.

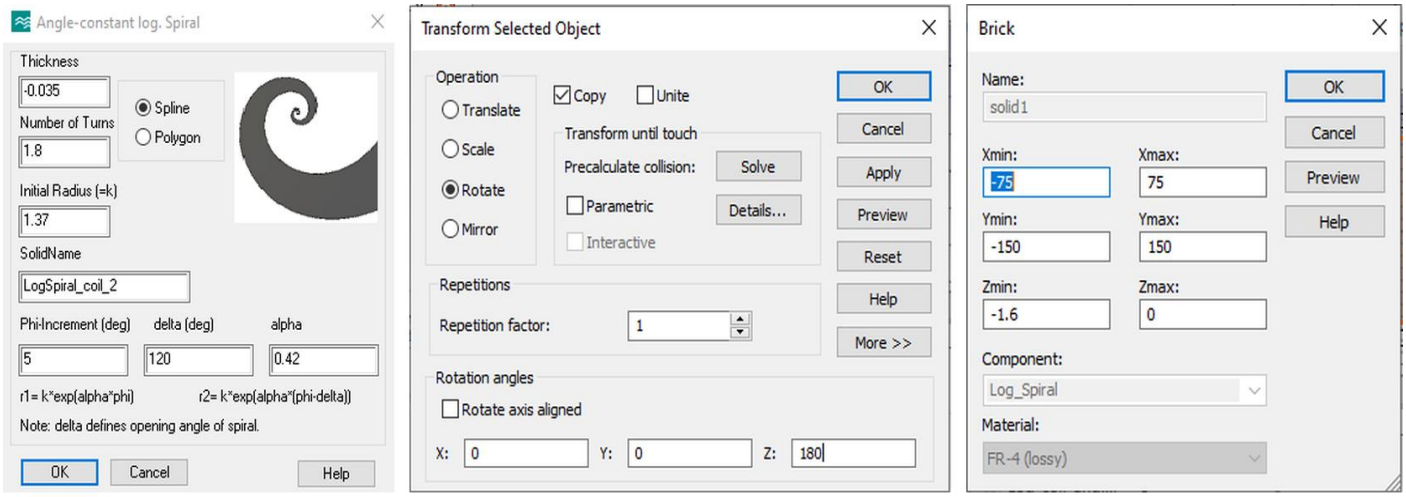

(a) (b) (c)

Fig. 2. CST implementation: (a) logarithmic spiral macro with the refined parameters, (b) 180° rotational copy for the second arm, (c) FR-4 substrate definition

From Analytical Seed to Refined Geometry

The seed parameters reported in [8] (k = 1.31 mm, α = 0.50, δ = 90°, N = 1.5) form a self-complementary spiral with rapid growth. The parameters actually simulated and fabricated, read from the CST parameter list, are k = 1.37 mm, α = 0.42, δ = 120° and N = 1.8. Table 1 compares the two sets using (5)–(7), and Fig. 3 plots both geometries directly from (1)–(2) against the board outline and the radius bounds.

Table 1. Analytical seed versus CST-refined parameters

Quantity	Seed [8]	Refined	Effect
Initial radius k (mm)	1.31	1.37	Both well inside r_{in} bound
Growth rate α	0.50	0.42	Slower radial growth
Arm angle δ (°)	90	120	Wider metal sector
Turns N	1.5	1.8	Termination rotated by 108°
Expansion per turn ε, Eq. (5)	23.1	14.0	39% lower
Arm edge ratio ρ, Eq. (5)	2.19	2.41	Wider arms

R_{max} (mm), Eq. (6)	145.8	158.4	Both exceed r_{out} = 95.5 mm
R_B (mm), Eq. (7)	66.5	65.7	Similar truncation edge
Fits 300 × 150 mm board	No (±146 mm across width)	Yes (tips at ±150 mm)	Board-compatible

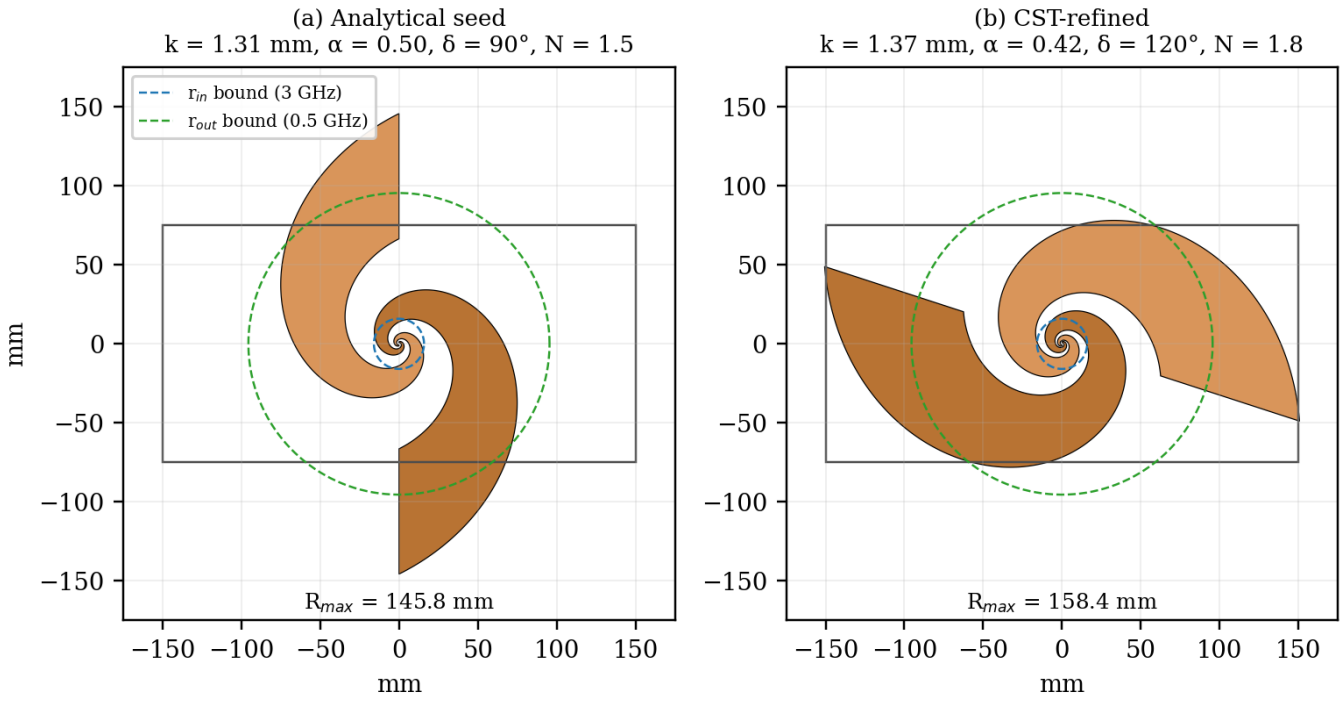

Fig. 3. Two-arm geometries computed from (1)–(2) for (a) the analytical seed and (b) the CST-refined parameters, shown against the 300 × 150 mm board outline and the radius bounds of (3)–(4)

Fig. 3(a) shows why the seed geometry could not be fabricated as computed. With N = 1.5 the arms terminate along the short axis of the board and reach ±146 mm, almost twice the 75 mm half-width available, so roughly half of each outer arm, which is the section responsible for the lowest frequencies, would have to be cut away. Reducing α from 0.50 to 0.42 lowers the per-turn expansion by 39%, so the spiral needs 1.8 turns to reach a comparable outer extent. The extra 0.3 turn rotates the terminations by 108° and places the arm tips at the long ends of the board, as in Fig. 3(b). The refined R_{max} of 158.4 mm still comfortably exceeds the 95.5 mm bound, and applying (4) in reverse to the termination radii (R_B to R_{max}) gives an estimated lower band edge of 0.30–0.73 GHz, which brackets the 0.5 GHz target. Because k = 1.37 mm lies far inside the 15.9 mm bound, the upper limit is set by the feed gap and connector rather than by the spiral itself.

The change in δ has an impedance interpretation. With δ = 120°, each 180° period contains 120° of metal and 60° of slot, so the structure is no longer self-complementary. By Babinet's principle [12], widening the metal relative to the slot lowers the input impedance below the 116–188 Ω range of (8), and the refined model gives a simulated input impedance of about 80 Ω [9]. Substituting 80 Ω into (9) with Z_0 = 50 Ω gives $|\Gamma|$ = 0.23, VSWR = 1.60 and S11 = −12.7 dB. This agrees closely with the simulated reflection floor of −12 to −14 dB and the VSWR of 1.5–1.7 observed across the simulated 1.8–5 GHz span [8], with a single resonant dip of −20.9 dB at 1.98 GHz. The residual mismatch is therefore mainly a resistive offset rather than a narrowband resonance, which indicates that a broadband transformer or tapered balun, rather than further tuning of α, is the natural next step toward a 50 Ω match.

In-House Fabrication Workflow

The refined layout was produced with subtractive photolithography on photoresist-coated, copper-clad FR-4, using equipment available in a university teaching laboratory. Table 2 lists the process steps and their parameters, and Figs. 4–6 show the equipment used.

Table 2. Fabrication process steps and parameters

Step	Equipment	Key parameters	Purpose
1. Photomask	Epson L210 piezoelectric inkjet	180 black nozzles, 3 pl droplets; AccuBlack water-resistant film; 1:1 artwork	Opaque mask of arm pattern
2. Exposure	UV exposure unit with vacuum frame	120 s; vacuum applied after lid closed	Harden resist under clear regions
3. Development	PA320 processor	Immersion developing	Reveal copper to be removed
4. Etching	Rota-Spray etcher; FAPC 3000 conveyor	Ferric chloride spray; < 90 s for 1 oz (35 µm) copper	Remove unprotected copper
5. Stripping	PA320 processor	Resist strip and rinse	Expose clean copper arms
6. Feed	Bench drill; soldering station	Hole at feed point; SMA soldered to both arm terminals	Connect 50 Ω coaxial port



Fig. 4. Mask and resist processing: (a) Epson L210 inkjet printer for the photomask, (b) UV exposure unit with vacuum frame, (c) PA320 processor for developing and stripping

The photomask is what most distinguishes this workflow from commercial PCB production. A consumer inkjet printer with 3 pl droplets resolves features far finer than the 1.14 mm feed gap, so resolution is not the limiting factor. Opacity matters more: each arm is a large continuous copper area, and any pinhole in the film becomes an unwanted opening, hence the dense water-resistant film. The vacuum frame keeps the film in intimate contact with the resist so that light does not spread under the mask edges during exposure. Mask quality remains the most accessible variable to refine (Section 6).



(a) (b) (c)

Fig. 5. Etching: (a) Rota-Spray processor with integrated spray-wash tank, (b) FAPC conveyorised processing line, (c) the developed spiral board entering the etcher

Spray etching removes 1 oz copper in under 90 s, and the short dwell time limits lateral undercut. Undercut matters most at the spiral centre, where the turns are densest (the second drawback identified in [9]) and where small gap changes alter the feed impedance. After stripping, the board was drilled at the feed point and an SMA connector was soldered so that its centre conductor and body contact the two inner arm terminals (Fig. 6). Centring this hole is critical, since an offset feed breaks the 180° symmetry of the model.



(a) (b)

Fig. 6. Feed assembly: (a) drilling the feed point at the spiral centre, (b) soldering the SMA connector

VERIFICATION SUMMARY

The fabricated antenna was characterised in [8] with a Keysight FieldFox N9915A analyser swept from 30 kHz to 9 GHz with 201 points, and its radiation pattern was measured at 2.75 GHz in an anechoic chamber. Table 3 consolidates those results with the simulation values discussed in Section 3.

Table 3. Consolidated simulated and measured performance (measured data from [8])

Metric	Simulated (CST)	Measured [8]
Minimum S11	−20.9 dB at 1.98 GHz	−32 dB
Minimum VSWR	1.198 at 1.98 GHz	1.0645

Reflection floor	−12 to −14 dB (1.8–5 GHz)	—
Deep return-loss dips	1.98 GHz	Near 0.65 GHz and 1.95 GHz
Continuous S11 ≤ −10 dB band	Whole simulated span (1.8–5 GHz)	About 1.0–6.1 GHz (VSWR = 2.01 at 6.16 GHz)
Below 1 GHz	Not simulated	Matched near 0.6–0.75 GHz; marginal (about −7.5 dB) near 0.8–0.95 GHz
Radiation pattern	Directivity pattern at 2.75 GHz	Measured at 2.75 GHz in anechoic chamber

Three observations link these results to the workflow. First, the measured dip near 1.95 GHz coincides with the simulated 1.98 GHz resonance, suggesting that the fabricated geometry reproduces the model closely. Second, the matched band extending to about 6 GHz is consistent with Section 3, where the small initial radius places the upper limit well beyond 3 GHz. Third, the match below 1 GHz is not continuous: it is good near 0.6–0.75 GHz but marginal around 0.8–0.95 GHz. This region lies just above the 0.30–0.73 GHz band-edge estimate, close enough to the lower limit that the truncated arms and finite board may still disturb the currents, and it was outside the simulated span used in [8]. Section 6 sets out how the workflow should address this.

CONCLUSION

This paper has documented the design-to-prototype workflow behind a previously reported ultra-wideband log spiral antenna for RF energy harvesting [8]. Closed-form radius bounds and three geometric checks show that the analytical seed geometry would have overflowed the 150 mm board width. Reducing α from 0.50 to 0.42 and increasing N from 1.5 to 1.8 lowers the per-turn expansion by 39% and fits the arms to a 300 × 150 mm board without compromising the lower band. Widening δ to 120° lowers the impedance toward 80 Ω, which explains the −12 to −14 dB simulated reflection floor. The prototype was made entirely with teaching-laboratory equipment, and the measurements of [8] confirm that this process reproduces the simulated geometry.

For future works, four directions follow. First, the full-wave sweep should be extended down to 0.5 GHz with the physical SMA connector modelled explicitly, so that the marginal 0.8–0.95 GHz region in Table 3 can be predicted rather than only measured. Second, a broadband impedance transformer or tapered balun should be simulated to bridge the 80 Ω antenna impedance and standard 50 Ω systems. Third, a practical rectifier, such as the Schottky voltage multipliers of [5], [7], should be integrated to quantify the DC power actually harvested under ambient conditions. Fourth, the inkjet mask parameters, such as print density, overlaid film layers and exposure time, should be optimised to improve edge definition and reduce pinhole risk around the dense central feed.

Declaration of prior publication

The prototype and its measured S11, VSWR and far-field results were first reported in [8]; both papers derive from [9]. Section 5 adds no new data. The analysis in Sections 2–3, the fabrication documentation and Figs. 1–6 are not part of [8].

REFERENCES

1. S. Shrestha, S. K. Noh, and D. Y. Choi, “Comparative study of antenna designs for RF energy harvesting,” Int. J. Antennas Propag., vol. 2013, Art. no. 385260, 2013, doi: 10.1155/2013/385260.

2. R. M. El Khosht et al., “A foldable textile-based broadband Archimedean spiral antenna for RF energy harvesting,” in Proc. Mediterranean Microwave Symp. (MMS), 2016, doi: 10.1109/MMS.2016.7803872.
3. W. Miao, Y. Delorme, F. Dauplay, G. Beaudin, Q. J. Yao, and S. C. Shi, “Simulation of an integrated log-spiral antenna at terahertz,” in Proc. 8th Int. Symp. Antennas, Propag. EM Theory (ISAPE), 2008, doi: 10.1109/ISAPE.2008.4735139.
4. S. Mandal and S. K. Giri, “Comparison of antennas for radio frequency energy harvesting in 0.2–2.4 GHz range,” in Proc. 3rd Int. Conf. Electron. Comput. Technol. (ICECT), vol. 1, pp. 93–97, 2011, doi: 10.1109/ICECTECH.2011.5941567.
5. H. Kumar, M. Arrawatia, and G. Kumar, “Broadband planar log-periodic dipole array antenna based RF-energy harvesting system,” IETE J. Res., vol. 65, no. 1, pp. 39–43, 2019, doi: 10.1080/03772063.2017.1385427.
6. K. Gangwar and J. Tissier, “Modified log periodic spiral antenna for multi-band RF energy harvesting applications,” in Proc. IEEE Wireless Power Transfer Conf. (WPTC), 2019, pp. 573–577, doi: 10.1109/WPTC45513.2019.9055540.
7. H. Jabbar, Y. S. Song, and T. T. Jeong, “RF energy harvesting system and circuits for charging of mobile devices,” IEEE Trans. Consum. Electron., vol. 56, no. 1, pp. 247–253, 2010, doi: 10.1109/TCE.2010.5439152.
8. N. B. Hassim and M. H. Iskandar, “Design and validation of an Ultra-wideband Log Spiral Antenna for RF Energy Harvesting,” International Journal of Research and Innovation in Social Science (IJRISS), Vol. IX, Issue X1 November 2025, DOI: 10.47772/IJRISS.
9. M. H. I. Mohamad Khairi, “Design and development of ultra wide band log spiral antenna for energy harvesting,” B.Eng.Tech. project report, Fac. Elect. Electron. Eng. Technol., Universiti Teknikal Malaysia Melaka, Melaka, Malaysia, 2021.
10. J. D. Dyson, “The equiangular spiral antenna,” IRE Trans. Antennas Propag., vol. 7, no. 2, pp. 181–187, 1959.
11. Y. Mushiake, “Self-complementary antennas,” IEEE Antennas Propag. Mag., vol. 34, no. 6, pp. 23–29, 1992.
12. H. G. Booker, “Slot aerials and their relation to complementary wire aerials (Babinet’s principle),” J. IEE Part IIIA: Radiolocation, vol. 93, no. 4, pp. 620–626, 1946.